CrossMark

Study on Texture Evolution and Shear Behavior of an Al/Ni/Cu Composite

Ali Shabani and Mohammad Reza Toroghinejad

The microstructure, texture, and mechanical properties of the Al/Ni/Cu composite during various accumulative roll bonding (ARB) cycles were studied using optical microscopy, scanning electron microscopy, x-ray diffraction, shear punch test, and hardness test. In addition, ImageJ software and Rietveld software were used in order to study microstructure and dislocation density variations, respectively. It was found that Ni and Cu layers were fractured and distributed in the Al matrix due to differences in their mechanical properties. Fracture and distribution of Cu and Ni particles after cycle five led to the alteration of the composite structure from a layered to a particle-reinforced structure. ARB process leads to the formation of strong orientation along the β-fiber and also to pronounced copper and dillamore components in both Al and Cu phases. Furthermore, the shear yield stress and ultimate shear strength of the composite increased as the ARB process advanced; however, shear elongation presented a non-uniform variation. Investigation of the fracture surfaces revealed that the mechanical properties of the composite are affected not only by the strain hardening of the Cu layer, but also by the structural change in the composite during the initial ARB cycles. During the last stages of the process, however, changes in mechanical properties were mostly governed by reinforcement particles serving as strain concentration zones and the strain hardening of the Al matrix.

1. Introduction

Metal matrix composites (MMCs), like all other composite materials, consist of at least two chemically and physically distinct phases that are suitably distributed to provide properties not obtainable with either of the individual phases alone. Generally, two phases; i.e., fibrous phase and particulate phase, are distributed in a metallic matrix (Ref 1, 2). The great interest in the production of these composites stems from their unique mechanical properties, such as low density, high electrical and thermal conductivity, wear resistance, and high formability. Most metal matrix composites are produced through squeeze or stir casting, spray forming, powder metallurgy techniques, or severe plastic deformation (SPD) processes (Ref 3-5). Among the different SPD methods, accumulative roll bonding (ARB) is the most common method for the production of ultrafine-grained (UFG) sheet metals and composites (Ref 6, 7).

Despite the large number of studies devoted to the mechanical properties of sheets and composites produced through the ARB process, the evaluation of the shear properties of these materials has been largely neglected (Ref 8-10). Therefore, we find it interesting to evaluate shear properties of composites produced via ARB process. However, Zabihi et al. (Ref 11) recently reported that shear strength of Al/Al$_2$O$_3$

composite improves by ARB process. It was seen that shear strength increases due to uniformity of reinforcements and decrease in porosity (Ref 11). In a different research, it was reported by Leon et al. (Ref 12) that particle size is an important parameter in shear properties of Al/Ni-SiC composite produced by infiltration of liquid aluminum into coated ceramics. In addition, Zabihi et al. (Ref 13) reported that shear strength of the Al/Al$_2$O$_3$ produced by ball milling and hot rolling decreases by increasing reinforcement amount.

Shear punch testing (SPT) is one of the most commonly used methods in scientific studies for the evaluation of the shear strength of materials (Ref 14, 15). This method may also be particularly useful in cases in which the material is only available as small test pieces or there are difficulties machining samples of extremely soft materials (Ref 16). Moreover, it is a promising method in weld joints, coatings, failed components, biomaterials, composites, and metallic glass, for which the use of conventional mechanical testing techniques is practically impossible (Ref 13, 14).

In this method, a sheet sample is placed between two die halves and a flat cylindrical punch is driven through the sample in order to punch out a circular disk from it. SPT curves similar to those obtained from uniaxial tension tests are then obtained by plotting load or shear strength versus normalized displacement. The curves thus obtained can then be used to derive such varied mechanical parameters as shear yield stress (SYS), ultimate shear strength (USS), and elongation values (Ref 15).

Due to different nature of SPT compared to tensile test, it seems attractive to evaluate mechanical properties of multilayered and particle-reinforced composites using this method. Therefore, the present study focused on the evaluation of shear properties of the Al/Ni/Cu composite produced via ARB and coating processes. SPT and hardness tests were also used to determine the mechanical properties of the composite during the different cycles of the ARB process. Finally, the

Ali Shabani and **Mohammad Reza Toroghinejad**, Department of Materials Engineering, Isfahan University of Technology, Isfahan 84156-83111, Iran. Contact e-mail: ali.shabani@ma.iut.ac.ir.

microstructure and fracture surfaces of the samples were studied using scanning electron microscopy (SEM).

2. Materials and Experimental Procedure

2.1 Materials and Processing

The materials used in this study included commercially pure Al and Cu strips annealed for 2 h at 663 K and 773 K, respectively. The Cu sheets were Ni-coated using an industrial electroplating process. The thickness of the Ni coating on the Cu strips after 120 min of electroplating was 30 μm, and the composite thus produced contained 3.75 wt.% of Ni. A maximum of 11 cycles of ARB were performed on three layers of Al/coated Cu/Al in order to produce the final Al/Ni/Cu composite. A complete description of the process may be found in studies by Shabani et al. (Ref 17, 18). In addition, during deformation the temperature was checked by a contact thermocouple in six different points. Temperature check was done on the samples from different cycles, and the average amount was reported as rolling temperature.

2.2 Investigation of the Structure, Texture, and Mechanical Properties

Formation of new phases during the process was investigated using an x-ray diffractometer (PHILIPS, the Netherlands) with Cu Kα ($\lambda = 0.15406$ nm) diffraction generated at 40 kV and 30 mA with the scanning angles ranging from 10° to 100°. Furthermore, the dislocation density of the samples subjected to different cycles of ARB was determined by analyzing the XRD patterns via the Rietveld software, Materials Analysis Using Diffraction (MAUD) (Ref 19). This method was used in different researches to characterize the microstructural parameters of different materials, including the calculations of the lattice parameter, phase percentage, crystallite size, and residual microstrain (Ref 20-22). The method is explained completely elsewhere (Ref 19, 21).

The microstructure of the Al/Ni/Cu composite in the RD–ND plane was observed using SEM to investigate the effects of the number of ARB cycles on composite structure. Furthermore, textures of the Al and Cu phases were analyzed using a SEM equipped with an electron backscatter diffraction (EBSD) attachment. The ideal orientations of texture components in FCC materials are shown schematically for the $\varphi_2 = 0°$, 45°,

and 65° sections of the ODF in Fig. 1. In addition, fractured layers were characterized in order to investigate the fracture behavior of the samples after SPT using a SEM (AIS 2300 Seron Technologies Inc., Korea) equipped with an energy-dispersive spectroscopy (EDS) operated at 20 kV.

In order to evaluate the mechanical properties of the composite, SPT was used at a crosshead speed of 0.2 mm/min at room temperature. The SPTs were performed on a Hounsfield testing machine (Model No. H25KS Hounsfield, UK) three times on each sample. The advantage of the punch device is that it can be constructed for any punch size. In this study, a punch of 3 mm in diameter and a die of 3.04 mm in diameter were used. Figure 2 shows a schematic illustration of the SPT process used.

The load–displacement data were converted to shear stress–displacement data using $\sigma = \frac{P}{\pi d t}$ equation (Ref 13, 23), where P is the punch load, t is the specimen thickness, and d is the average diameters of the punch and the die. $\left(\frac{n_\tau}{0.002}\right)^{n_\tau} = \frac{\tau_{USS}}{\tau_{SYS}}$ and $\varepsilon_u = 2.26 n_\tau - 0.15$ equations were used to calculate shear elongation using SPT results (Ref 23), where ε_u is the uniform shear elongation, n_τ is the strain hardening exponent in SPT, and τ_{SYS} and τ_{USS} represent shear yield stress and ultimate shear stress, respectively.

Vickers hardness of the samples on the RD–TD plane was also measured under a load of 5 kg. For each sample, eight tests were performed, the abnormal off points were deleted, and the average of the remaining points was reported as sample hardness value.

3. Results and Discussion

3.1 Microstructural and Texture Evaluation

Figure 3 presents the SEM and OM micrographs of the microstructure of the composite samples on the RD–ND plane after cycles zero, five, and eleven of the ARB process. Generally, necking and fracture occurred in the harder layers of the multilayered composites due to differences in the flow and mechanical properties of the layers (Ref 10). Hardness values of 25, 50, and 150 HV were obtained for Al, Cu, and Ni, respectively. As expected, the Al layers retained their coherence in most regions during the ARB process.

As the process advanced, it was observed that Ni layers followed by the Cu layers necked, fractured, and were
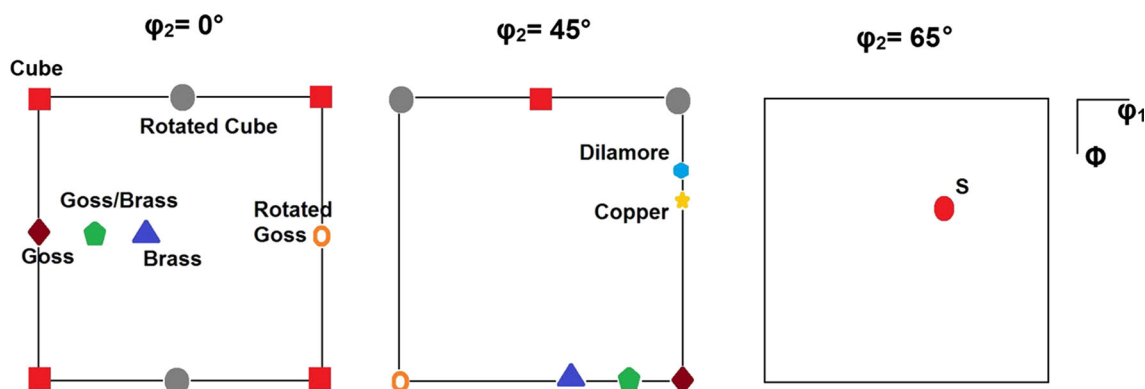

Fig. 1 Schematic illustration of the important texture components in FCC materials

distributed in the Al matrix. Finally, after eleven cycles, a quite uniform composite was produced with a homogeneous distribution of Cu and Ni particles in the Al matrix (Fig. 3a, b, c, d, e, and f). It is also clear from Fig. 3(a) and (e) that the structure of the composite changed during the process, and the composite exhibited a layered structure during the initial cycles, but demonstrated a particle-reinforced structure at the end of the process.

The number and average size of the particles in a 1×1 mm surface area of the RD–ND plane of the samples were measured using ImageJ software (Fig. 4). Evidently, the number of the particles in the composite structure increased as the process proceeded due to the fracturing of the Cu and Ni layers. In the primary cycles of the ARB process, the composite exhibited a layered structure. During the process, however, the structure of the composite changed to a particle-reinforced structure as judged from the distribution and fracturing of the Cu and Ni layers in the Al matrix. According to Fig. 4, the number of particles increased considerably after cycle five, while the particle size in the matrix reduced during the process. Moreover, a rapid decrease is observed in this figure in the average size of the Cu layers during the primary cycles. At higher cycles, however, the average particle size approached less than 200 μm, but its decreasing rate declined. The significant increase in the number of particles and the average particle size of less than 3000 μm² after five cycles indicate the shift in the composite structure from a layered to a particle-reinforced structure. These structural changes in the composite can strongly affect mechanical properties.
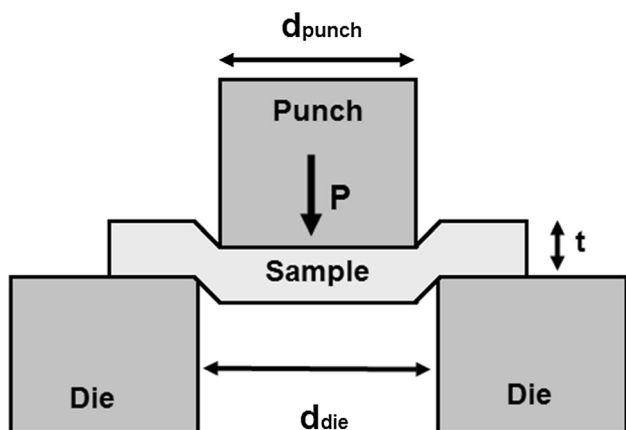

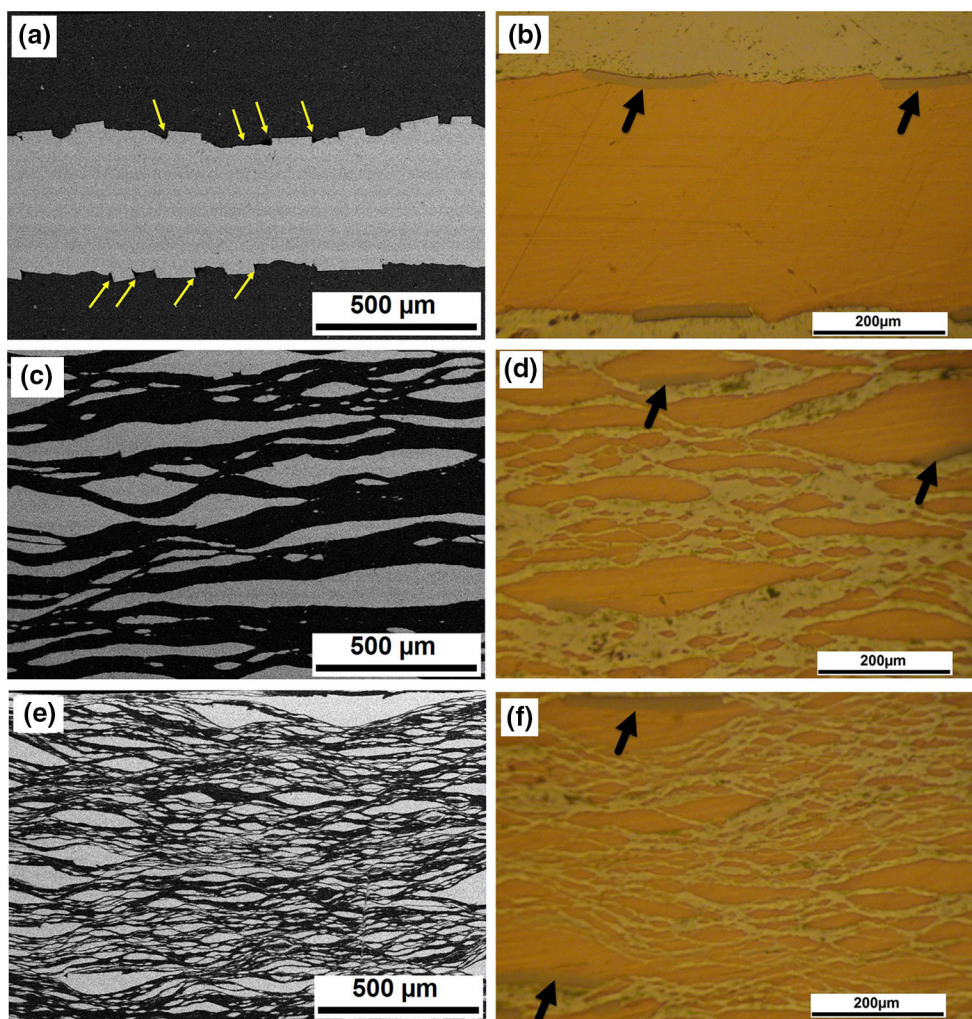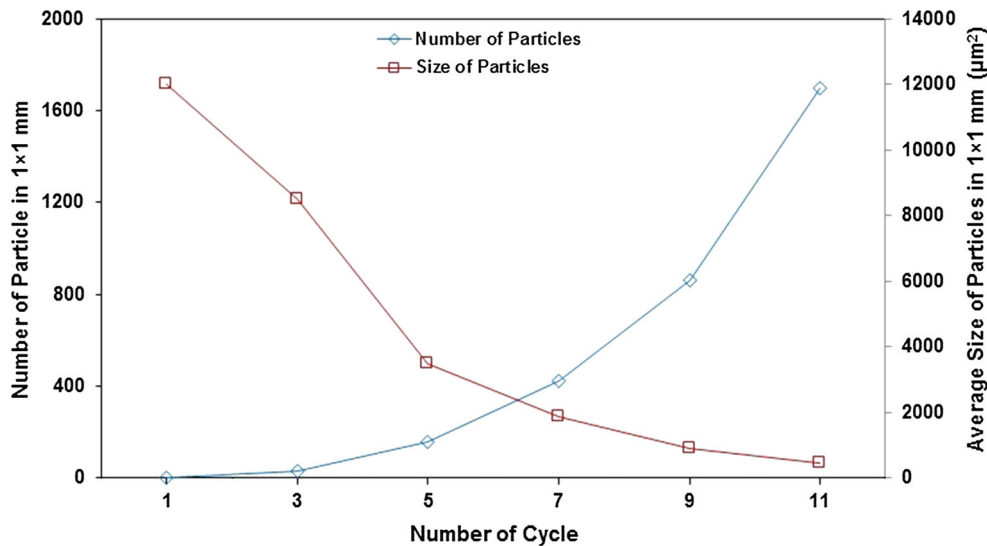**Fig. 2** Schematic illustration of the shear punch device

Fig. 3 Microstructure of the composite on the RD–ND plane after (a) and (b) cycle zero, (c) and (d) cycle five and (e) and (f) cycle eleven

Fig. 4 Variations in the number and average size of particles in a 1×1 mm surface area RD–ND plane of the composite in different ARB cycles

Generally, the formation of new compounds with the elements in the composite significantly affects its mechanical properties (Ref 17, 24). Figure 5(a) shows typical x-ray diffraction (XRD) patterns of a 1×1 cm^2 surface area of the RD–TD plane of the composite after different cycles. Based on the XRD data, only the Al and Cu phases were present in the composite, which indicates that no detectable reaction took place among Al, Ni, and Cu during the deformation process. On the other hand, Fig. 5(b) reveals the composition profile across the Cu-Ni-Al interface after eleven cycles of ARB process, as obtained by EDS line scan analysis. It can be seen that no significant diffusion of the elements happened at the interface after eleven cycles of ARB. Therefore, it can be said that no detectable reaction took place among Al, Ni, and Cu during the deformation process.

Figure 6 demonstrates the $\varphi_2 = 0°$, $45°$, and $65°$ sections of the ODFs of the Al phase with increasing ARB cycles. It can be seen that brass and rotated goss (rt-goss) are the main texture components of the Al phase after one cycle of ARB; however, weak components of rotated cube (rt-cube) and S are also evident. As shown in Fig. 6(b) after five cycles of ARB the rt-goss and S components disappear and rt-cube and brass components become stronger. Moreover, a goss component forms after this cycle. Figure 6(c) presents that after nine cycles of ARB the rt-cube, copper, and dillamore are the major texture components and other components disappear. The intensity of rt-cube, copper, and dillamore components increases by improving ARB process to the eleventh cycle (Fig. 6d); however, a weak brass component is also formed in this cycle.

The $\varphi_2 = 0°$, $45°$, and $65°$ sections of the ODFs of the Cu phase with increasing ARB cycles are revealed in Fig. 7. Cube, brass, and goss/brass are the major texture components after the first cycle. After five cycles of ARB, the goss/brass component disappears and the brass component weakens; however, cube component becomes stronger. As shown in Fig. 7(c), improving the process to the ninth cycle leads to formation of new components such as copper, dillamore, goss, and goss/brass. In addition, cube component disappears and the brass becomes stronger after this cycle. The overall intensity of the components after the eleventh cycle indicated a remarkable increase

compared to the previous cycles (Fig. 7d). Copper, dillamore, and S components become stronger, whereas goss and goss/brass eliminate completely and brass remains almost stable.

The variation of maximum intensity versus the number of ARB cycle for the Al and Cu phases for various texture components is presented in Fig. 8(a) and (b), respectively.

It can be seen that in Al phase, the copper, dillamore, and rt-cube components intensify, remarkably by increasing ARB cycles (Fig. 8a). However, components such as goss, rt-goss, and brass weaken or disappear completely during the process. In addition, as shown in Fig. 8(b) in Cu phase the copper, dillamore, and S components become stronger significantly by increasing ARB cycles, while cube, goss/brass, and brass components weaken or disappear by improving the ARB process.

As explained above, copper, dillamore, and rt-cube components intensify during the ARB process and are the main texture components of Al phase after eleven cycles of ARB. Formation of these components during cold deformation of Al was reported in different researches (Ref 25, 26). Shear bands formation during cold rolling of Al was proposed as the main reason of shear texture (rt-cube) formation (Ref 25, 26). As Toroghinejad et al. (Ref 27) reported, the number of shear bands increased with the ARB cycles resulting in increase in the rt-cube intensity. In addition, Raei et al. (Ref 25) reported that during the ARB process when the material at the surface is cycled into the center after each pass and is subjected to a pure plane strain compression, the surface shear texture component rotates toward a single copper rolling component. This single component will then again rotate toward a shear texture as it subsequently moves outwards the surface. This cyclic ratcheting thus leads to the increase in the intensity of the copper component and surface shear component (rt-cube).

In addition, it was seen that the copper, dillamore, brass, and S are the main texture components of the Cu phase after eleventh cycle of the ARB. Formation of these components during cold deformation of Cu was also reported in different researches (Ref 26, 28, 29). Generally, copper, S, and brass are the main texture components of deformed high- and medium-SFE materials (Ref 28, 30), and shear banding and deformation
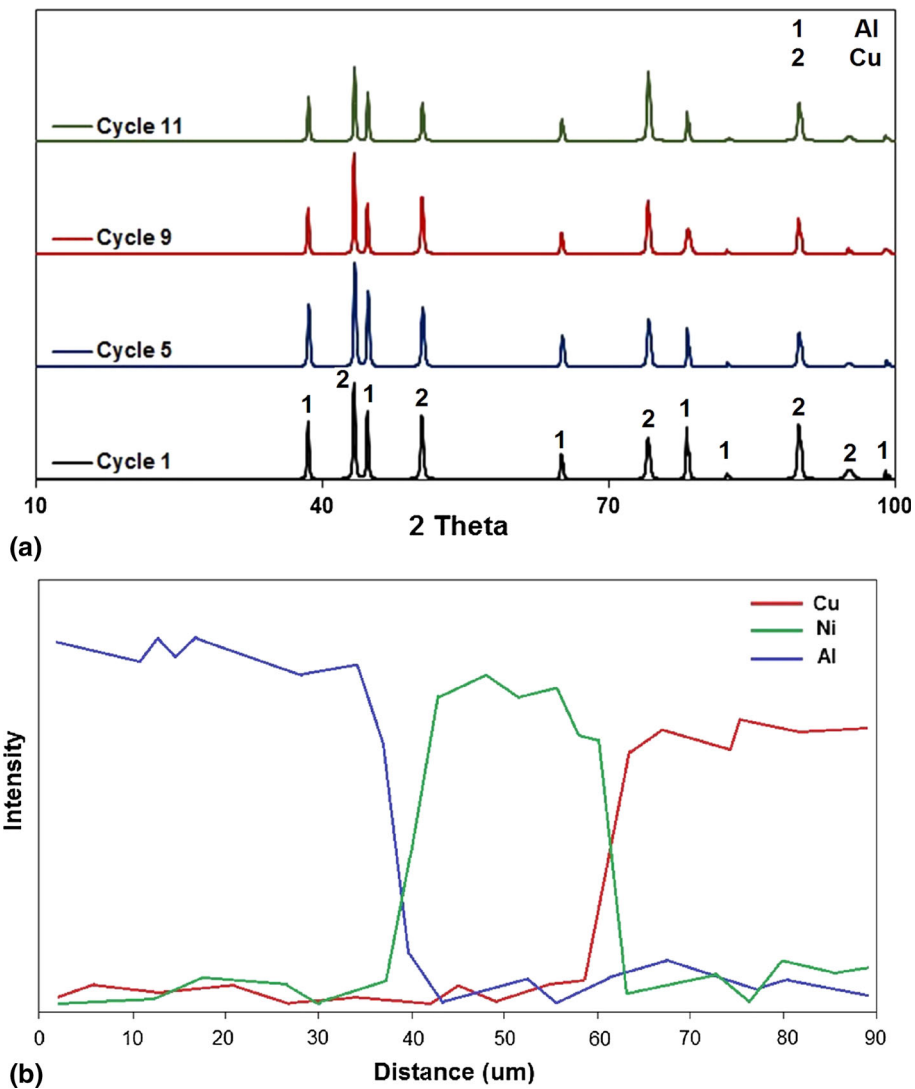
Fig. 5 (a) XRD patterns of the composite after different cycles and (b) EDS line scan at the interface of Cu-Ni-Al layers after eleven cycles

twining are reported as the dominant mechanisms for the formation of these components (Ref 29). Additionally, Torogh-inejad et al. (Ref 27) claimed that formation of β-fiber texture which runs from the brass orientation through the S orientation to the copper orientation is related to the dislocation structures introduced during the ARB process. According to their report, with increasing the ARB cycles the stored energy of deformation and the strain hardening of the material increase. Therefore, the spacing between dislocation cells boundary and the intensity of the β-fiber texture (brass, S, and copper components) increase (Ref 25-27).

3.2 Mechanical Properties and Fractography

The mechanical behavior of the multilayered composite produced through ARB process was evaluated using SPT. The results obtained for different cycles are presented in Fig. 9, in which force is plotted versus normalized displacement. Evidently, the shear force of the composite improved with increasing number of ARB cycles.

Variations in the SYS, USS, and shear elongation of the Al/Ni/Cu composites versus the number of ARB cycles are shown

in Fig. 10. It is clear from this figure that SYS and USS increased in the composite with increase in the number of cycles. The enhancements observed in the strength of the composite during the ARB process are in line with the findings reported in previous studies (Ref 4, 9, 10). Furthermore, SYS values increased from 95 to 150 MPa after eleven ARB cycles, indicating an enhancement of 63%. However, increase in SYS value was observed between cycles zero to one and five to seven in which the maximum variation rate of more than 10% per cycle also occurred. Nevertheless, the USS value of the composite increased at an almost constant rate of 4% per cycle during the whole process as evidenced by a gradual increase from 132 MPa after the primary sandwich to 185 MPa after the eleventh cycle. Zabihi et al. (Ref 11) reported almost 30% increase in USS of Al-Al2O3 composite through ARB process. The reinforcing role of alumina particles, uniformity of alumina particles, and decrease in porosity content were reported as the main reasons for this enhancement. Tensile and bending properties of the Al/Ni/Cu composite were investigated in a study by Shabani et al. (Ref 9). In Fig. 11(a) and (b), USS variation is compared with the variations of the ultimate tensile strength (UTS) and bending strength (BS) of the composite. It
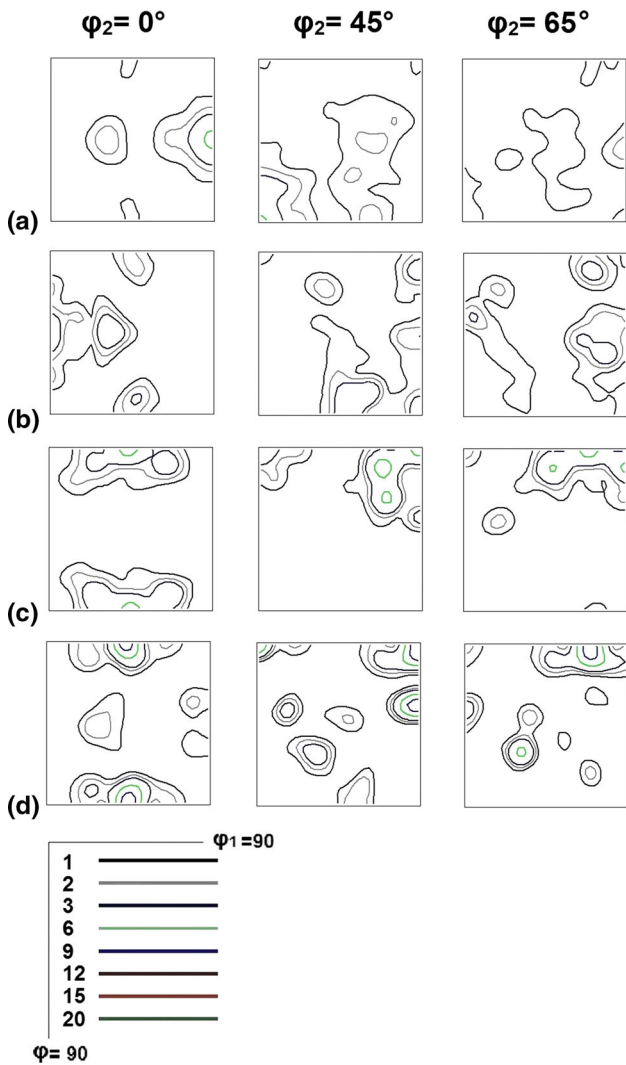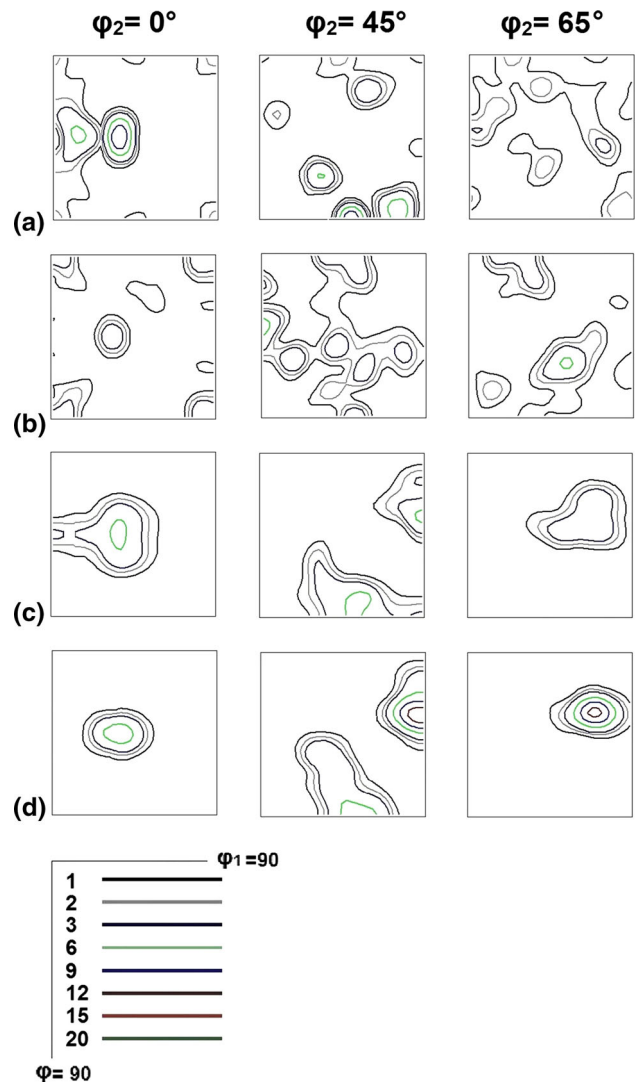
Fig. 6 The $\varphi_2 = 0°$, 45°, and 65° sections of the ODFs of the Al phase after cycle (a) one, (b) five, (c) nine, and (d) eleven

Fig. 7 The $\varphi_2 = 0°$, 45°, and 65° sections of the ODFs of the Cu phase after cycle (a) one, (b) five, (c) nine, and (d) eleven

can be seen that the increase rate of the USS and UTS are almost the same; however, these rates change after cycle five. Almost the same thing happens to USS and BS variations (Fig. 11b). Therefore, two results can be concluded from these figures. (1) As the USS, UTS, and BS of the composite revealed almost the same behavior during the ARB process, it can be concluded that the mechanisms govern the UTS and BS enhancement, and are also effective in USS increase. (2) And shear strength, the UTS, and BS of the composite are sensitive to the microstructure change after cycle five of ARB.

Figure 10 also shows that the shear elongation of the composite decreased as a result of the ARB process. As can be seen, shear elongation decreased from 4 to 1.2% after eleven cycles. Moreover, this variation was non-uniform throughout the process with the highest rate of decrease occurring between cycles zero and one and seven and eleven. However, an enhancement in shear elongation was observed between cycles one to three.

It is a point of common agreement (Ref 4, 6) that variations in the tensile strength and elongation during the ARB process are governed by strain hardening due to dislocations and grain refinement. However, as reported in previous studies (Ref 8-

10), in addition to these two mechanisms, some other factors are effective on mechanical properties' variations. The following parameters may be involved in the changes observed in the strength and elongation of Al/Ni/Cu composites during the ARB process.

1. Reduced dislocation motions and the generation of new dislocations due to the presence of Cu and Ni reinforcement. Using $\rho = \frac{2\sqrt{3}\cdot\varepsilon}{Db}$, equation dislocation density (ρ) of the samples could be measured (Ref 20), where ε is the microstrain, D is the crystallite size, and b is the Burgers vector ($b = a/\sqrt{2}$ for the FCC structure where a is the lattice parameter). Crystallite size (D) and microstrain (ε) of the alloy at different ARB cycles were calculated using MAUD software and XRD patterns. Figure 12 reveals the calculated D parameter for the Al and Cu phases in different ARB cycles. Furthermore, Fig. 13 reveals the variation in microstrain and dislocation density for the Al and Cu. Microstrain increases by ARB cycle for both the phases; however, a decrease in microstrain of Al can be seen between cycles 5 and 7,
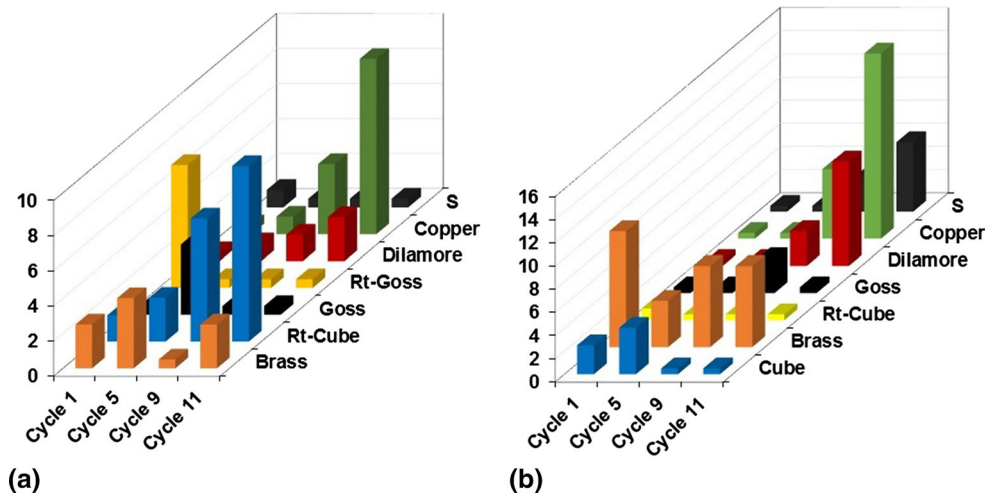
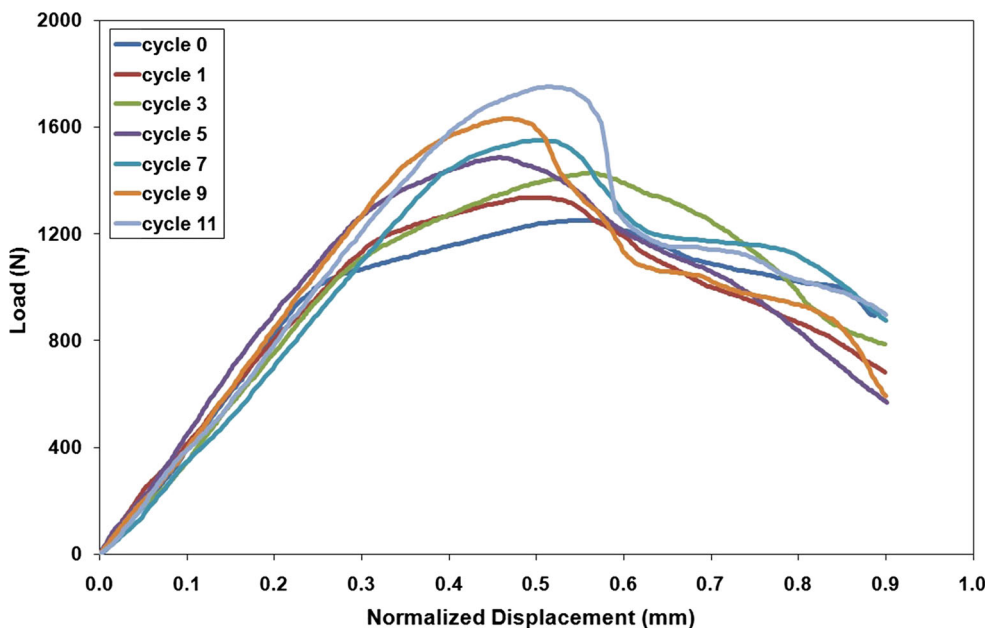**Fig. 8** Variation of maximum intensity versus the number of ARB cycles for (a) Al and (b) Cu phases

Fig. 9 SPT curves for composites after different cycles

which can be attributed to the recovery of Al. Dislocation density also increases by proceeding ARB process for both the phases. Increasing rate of dislocation density reduces after cycles 5 and 7 for the Al and Cu, respectively, due to recovery and also the saturation of dislocation in structure.

2. Enhanced uniformity of reinforcement size and distribution as the process proceeds. Size and number of particles besides microstructure can be used to show uniformity of particle distribution. Using ImageJ software, particle size distribution in Al matrix was evaluated for different ARB cycles. It is important to point out that, in the cycle zero, the Cu layer was considered as a particle. As shown in Fig. 14, particle size decreases through ARB and after eleven cycles more than 60% of particles have the size less than 60 μm^2. Decrease in particle size and enhancement in number of particles as shown in Fig. 4 besides microstructure of composites (Fig. 3) re-

veal the enhancement in uniformity of particle size and distribution. Enhancement in uniformity leads to increase in particle distance as well as crack path before failure.

3. Increased bonding quality between the reinforcement and the matrix during the ARB process. As shown by arrows in Fig. 3(a), bonding quality between layers is low at primary cycles. However, by increasing ARB cycle bonding quality improves due to applied rolling pressure, and consequently crack initiation decreases in the interfaces.

4. The mismatch between the coefficients of thermal expansion (CTEs) of the matrix and the reinforcements may also be effective in the shear strength variation of strip composites (Ref 13). During the ARB process, the temperature of the sample generally increases (almost 200 K) due to the plastic deformation and the friction between the roller and the sample (Ref 4, 6). Therefore, mismatch of CTEs of Al, Ni, and Cu (23, 13, and 50 mm/mK, respectively) (Ref 31) will then lead to almost 0.0074
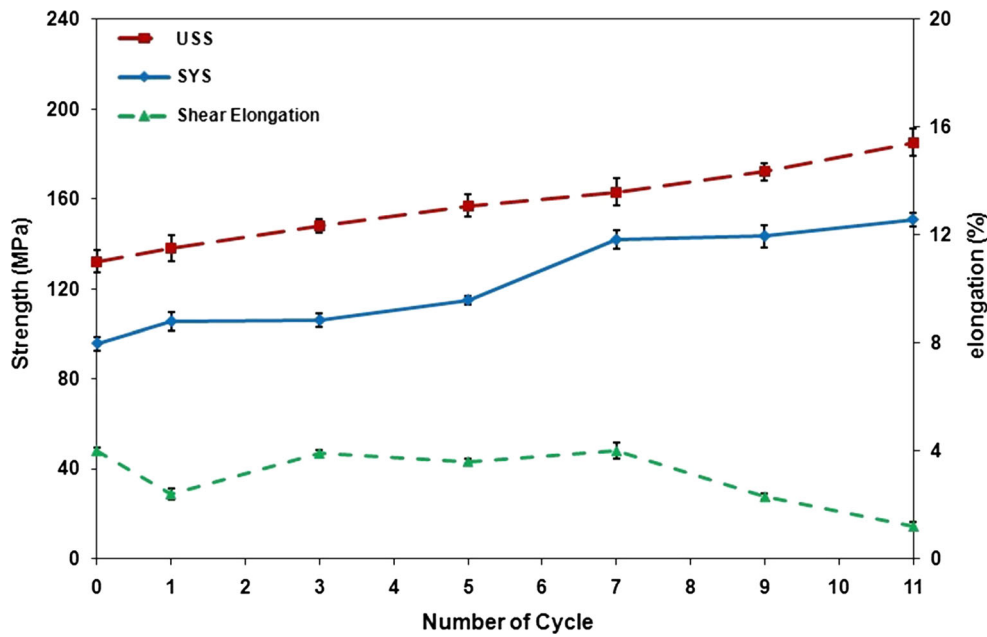
Fig. 10 Variations in the mechanical properties (USS, SYS, and shear elongation) with increasing number of ARB cycles
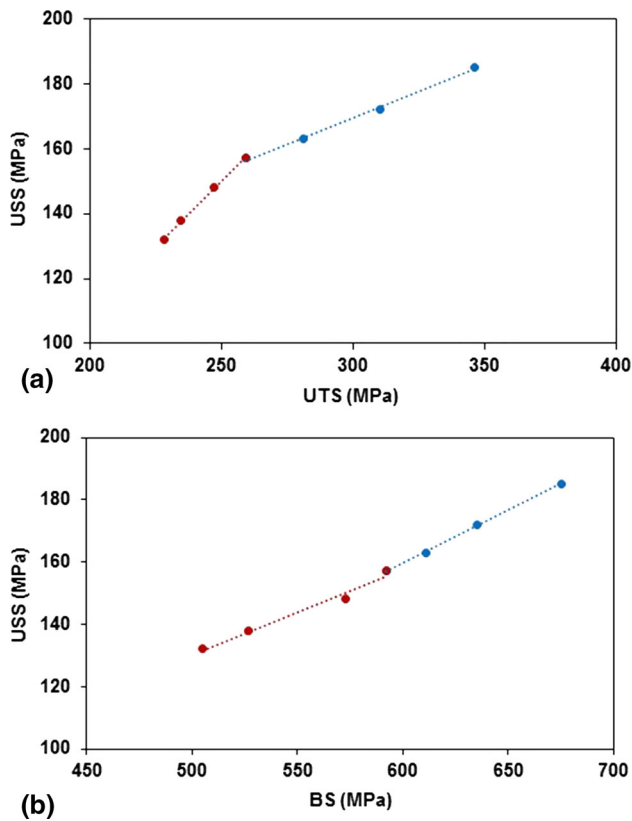

Fig. 11 Shear strength variation vs. (a) UTS and (b) BS variation (Ref 9)

Fig. 12 Calculated crystallite size of the Al and Cu in different ARB cycles

As previously mentioned, the maximum rate of increase in SYS was observed between cycles zero and one, and five and seven. This high rate of increase in SYS after the first cycle is due to the large amount of strain hardening during deformation (Ref 4, 6). However, the increasing rate of SYS enhancement after cycle five may be attributed to the composite structure. As shown in Fig. 3 and 4, composite structure changes from a layered structure to one of particle-reinforced structures after cycle five. Ni and Cu particles play a major role in decreasing the dislocation motion and the generation of new dislocations in the composite, thereby leading to increase in SYS values after cycle five.

In addition, as explained above, variation of shear elongation is non-uniform during the process and cannot be explained by these parameters alone. To shed more light on the real underlying causes of the fluctuations in shear elongation during the ARB process, the fracture surface of the punched-out SPT disks was examined. This revealed three main Al/Cu/Al layers

and 0.002 strain around Cu and Ni particles, respectively (considering particles with 100 μm length), and, consequently, the generation of new dislocations at the interfaces of the components. This rise in temperature is one of the factors involved in the increase in shear strength of the composite during the ARB process (Ref 13).
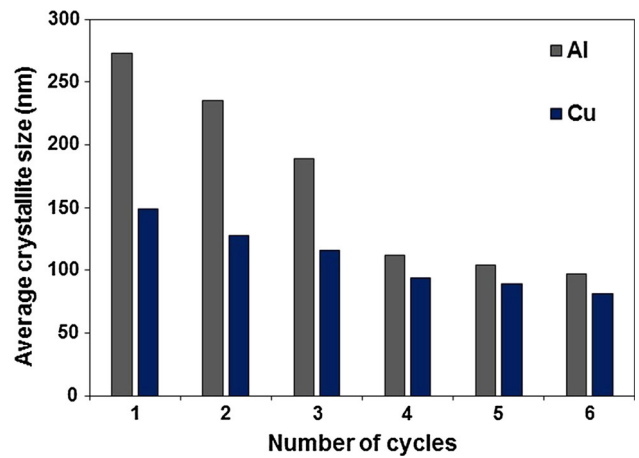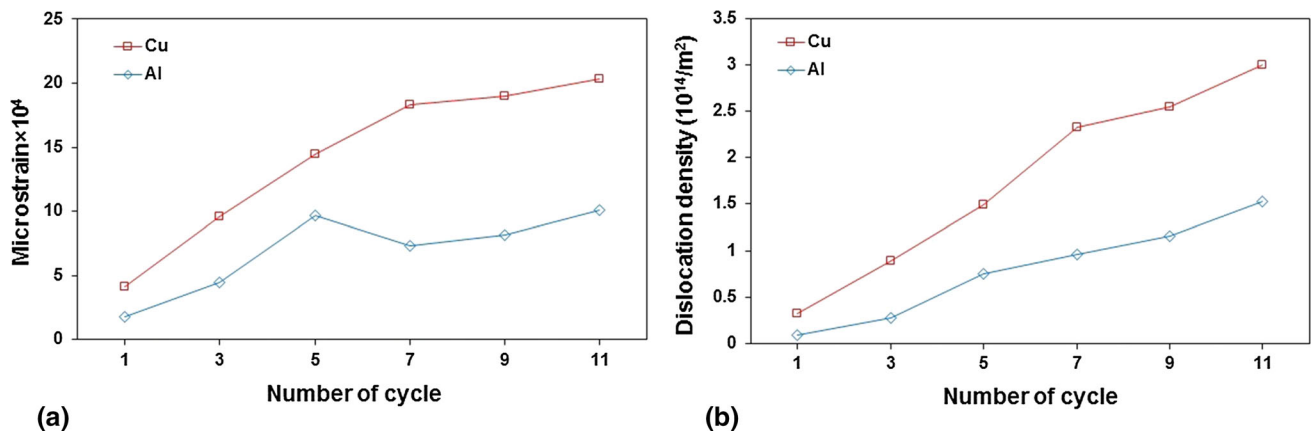
Fig. 13 (a) Microstrain variation and (b) dislocation density variation with ARB cycle
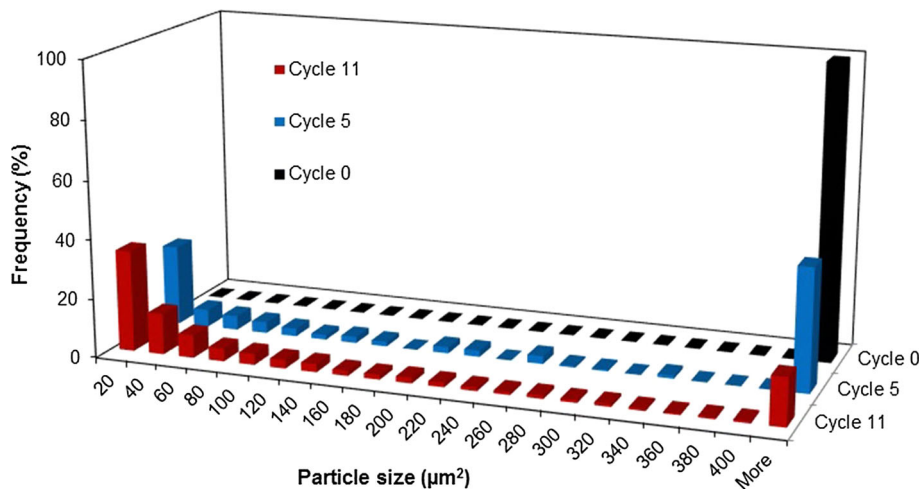

Fig. 14 Particle size distribution in different ARB cycles

in the sample after the primary cycle (Fig. 3a). In the SPT, the outer layers (i.e., the Al layers) receive maximum force during the punching process and would, therefore, be fractured before the interior layers (i.e., Cu layers) (Fig. 15a, b, and c). Consequently, elongation is more dependent on the Cu layer and its maximum amount is observed in this layer due to the uniformity of the Cu layer and the low amount of strain hardening in the composite. Furthermore, Fig. 15(b) reveals a typical ductile fracture in both the Al and Cu layers. As shown in Fig. 10, shear elongation of the composite declines rapidly after the initial cycle. Applying a strain of about 0.7 to the composite results in dislocation hardening in the composite layers, especially in the Cu layer, due to the smaller stacking fault energy of Cu compared to that of Al layers (Ref 9). The Cu layers, therefore, go through more strain hardening than the Al layers. The high rate of strain hardening in the Cu layer observed after the initial cycles resulted in a decrease in the shear elongation of the composite.

Cu layers are only coherent in the primary cycles, but subsequently start to neck and fracture locally (Fig. 3b and c). Therefore, shear elongation is more dependent on the Al matrix than on the Cu particles in the composite with the new structure as compared to the layered composite produced after primary cycles. Based on the higher formability and lower strain

hardening of Al, the variation in the structure of the composite after the primary ARB cycles and the dependency of elongation on Al may be presented as the main reasons for the increased elongation in the mid-cycles of the process.

Figure 15(d) to (f) illustrates the fracture surface of the composite after five cycles of the ARB process. Evidently, the Al matrix reveals a ductile behavior; however, the size and number of dimples have decreased compared to what is seen in Fig. 15(b). In addition, a rupture has occurred in the inner layers in the presence of Cu particles.

In the final stages of the process, Cu and Ni layers fracture and separate and, thus, give rise to an increment in the number of reinforcements in the matrix and an enhancement in their hardening effect. Shear elongation, therefore, decreases from cycle seven to eleven due to the increased hardening effect of the reinforcement and strain accumulation. EDS results and fracture surface images of the composite after eleven cycles are presented in Fig. 15(g), (h), and (i). It can be seen that the Al matrix does not reveal a ductile behavior in this cycle; rather, it has a mostly brittle fracture.

Evidently, the depth and size of the dimples changed with the increasing number of ARB cycles. This represents a change in the failure mechanism of the samples. Figure 15(h) shows dimples with significantly reduced size and depth, indicating a

change in the fracture mechanism from a ductile to a shear ductile fracture. Furthermore, it is clear from Fig. 15(g), (h), and (i) that fracture occurred near the second phases due to strain concentration in these zones.

Briefly, shear elongation decreases in the final cycles of the ARB process as a result of dislocation hardening which occurs due to both strain accumulation during the ARB process and the presence of Cu and Ni reinforcement particles serving as strain concentration zones.

Figure 16 shows the variations in the hardness of Al/Ni/Cu composite during the ARB process and those of pure Cu and Al. A remarkable increase is observed in hardness values after one ARB cycle; this increase is almost 2 times greater than that of the annealed Al. The rapid increase in hardness during the primary stages seems to be related to strain hardening, similar to the increase in strength explained above. After cycle zero, hardness rapidly increased, then dwindled, and was finally saturated by further rolling. This is consistent with the observations reported in other studies on the ARB process (Ref 32, 33). This can be related to the continuous decrease in strain hardening during plastic deformation. The rate of enhancement in hardness further increased again after cycles five to nine. In this work, hardness measurements were performed on sample surfaces. As a result, the effect of reinforcement is not taken into account up to a specific (fifth) cycle. After the fifth cycle, however, hardness increased rapidly due to changes in the composite structure and the reinforcing effects of Ni and Cu particles in the Al matrix (i.e., additional strain hardening). Figure 16 also shows that the hardness value of MMC increased from 26 to 99 HV (a 360% increase) after eleven ARB cycles.
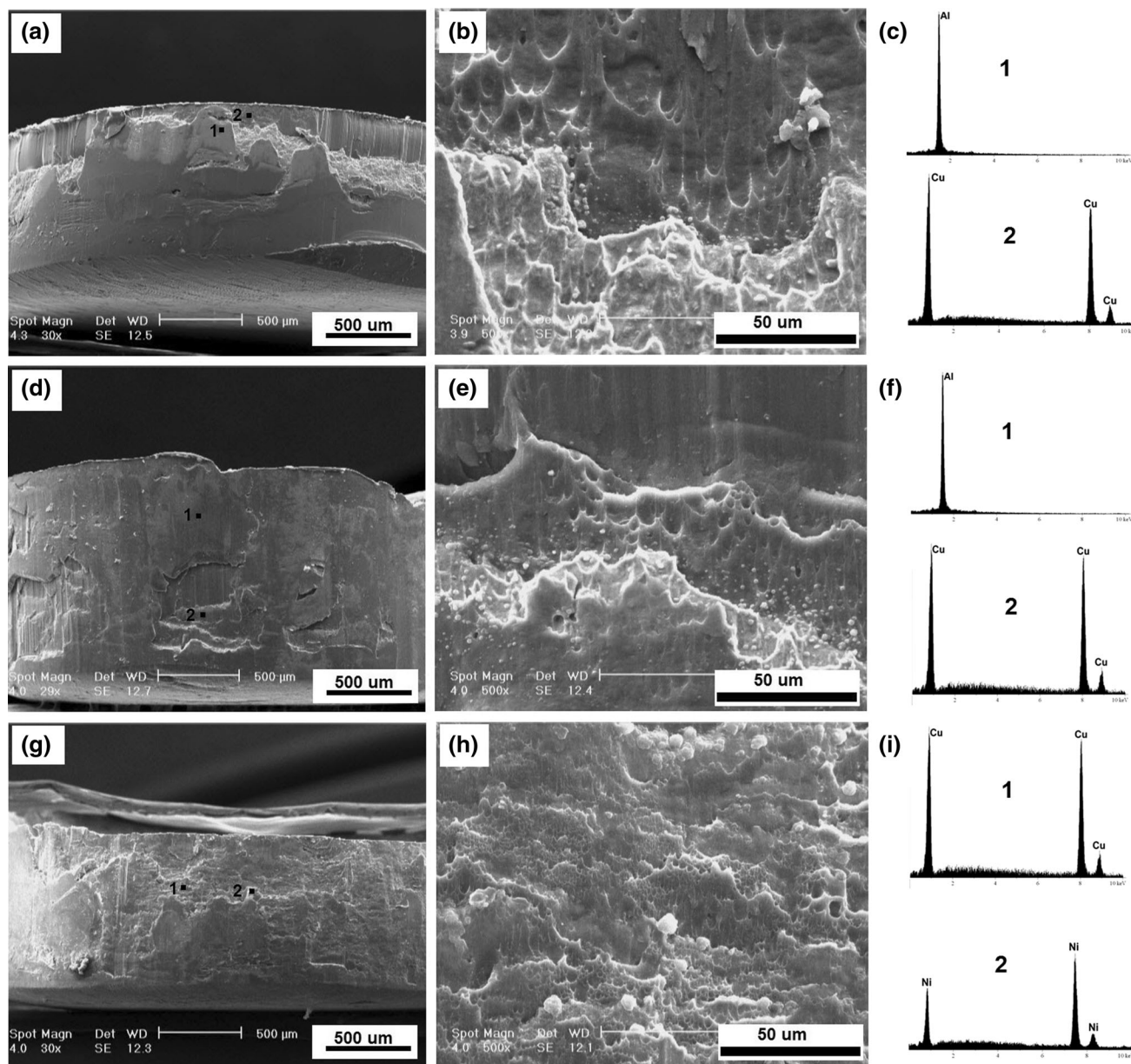
Fig. 15 EDS analysis and SEM micrograph of fracture surfaces of composites (a, b, and c) after cycle zero, (d, e, and f) after cycle five, and (g, h, and i) after cycle eleven
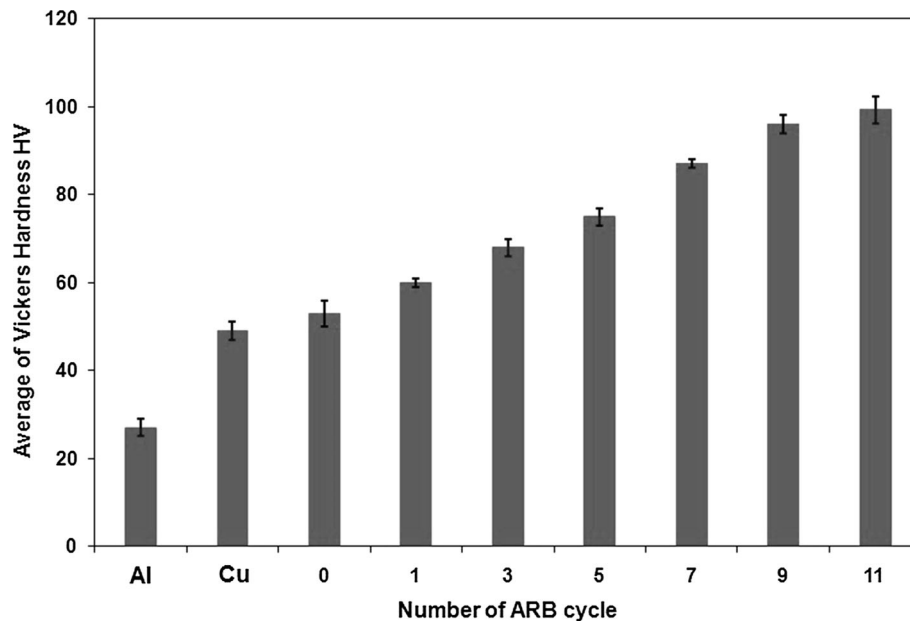
Fig. 16 Variations in the hardness of Al/Ni/Cu composite subjected to different ARB cycles and those of pure Al and Cu

4. Conclusions

In this work, the mechanical properties of the Al/Ni/Cu composite were evaluated using SPT. Microstructural observations and EDS analysis were used to study the variations in mechanical properties and to investigate the fracture mechanisms involved. The following conclusions may be drawn from the findings of this study:

1. Fracturing of Ni and Cu layers during the ARB process led to the formation of an Al/Ni/Cu composite with a uniform distribution of reinforcements after eleven cycles.
2. Variations in the size and number of particles revealed that the composite structure underwent a change from a layered to a particle-reinforced structure after five cycles of ARB.
3. The intensity of rt-cube, copper, and dillamore components increased by improving ARB process to the eleventh cycle in Al phase. However, in Cu phase the copper, dillamore, and S components become stronger significantly by increasing ARB cycles, while cube, goss/brass, and brass components weaken or disappear by improving the ARB process.
4. SPT revealed that SYS and USS of the composite increased steadily as the ARB process advanced. It was observed that eleven cycles of the process brought about an enhancement in SYS of about 60% and an increase in USS of more than 40%. Variations in shear elongation during the process, however, were non-uniform.
5. SEM fractographs of the fracture surfaces showed that elongation during the primary cycles of the ARB process is controlled not only by the strain hardening of the Cu layer, but also by the changes in the composite structure from a layered to a particle-reinforced structure. Furthermore, variation in shear elongation during the final stages of the process was mostly governed by the effect of rein-

forcement particles as strain concentration zones and the Al matrix strain hardening.
6. The MMC thus produced exhibited a higher hardness than annealed Cu and Al. This enhanced hardness was attributed to the strain hardening of the Al layer in the primary cycles and the reinforcement in the Al matrix after cycle five.

References

1. N. Chawla and K.K. Chawla, *Metal Matrix Composites*, Springer, Berlin, 2006
2. P. Cavaliere, B. Sadeghi, and A. Shabani, Carbon Nanotube Reinforced Aluminum Matrix Composites Produced by Spark Plasma Sintering, *J. Mater. Sci.*, 2017, **52**(14), p 8618–8629
3. P.K. Rohatgi, Cast Aluminum—Matrix Composites for Automotive Applications, *JOM*, 1991, **43**, p 10–15
4. N. Tsuji, Y. Ito, Y. Saito, and Y. Minamino, Strength and Ductility of Ultrafine Grained Aluminum and Iron Produced by ARB and Annealing, *Scr. Mater.*, 2002, **47**, p 893–899
5. P. Cavaliere, F. Jahantigh, A. Shabani, and B. Sadeghi, Influence of SiO2 Nanoparticles on the Microstructure and Mechanical Properties of Al Matrix Nanocomposites Fabricated by Spark Plasma Sintering, *Compos. B Eng.*, 2018, **146**, p 60–68
6. Y. Saito, N. Tsuji, H. Utsunomiya, T. Sakai, and R.G. Hong, Ultra-Fine Grained Bulk Aluminium Produced by Accumulative Roll-Bonding (ARB) Process, *Scr. Mater.*, 1998, **39**, p 1221–1227
7. M. Reihanian, S. Fayezipour, and S.M. Lari Baghal, Nanostructured Al/SiC-Graphite Composites Produced by Accumulative Roll Bonding: Role of Graphite on Microstructure, Wear and Tensile Behavior, *J. Mater. Eng. Perform.*, 2017, **26**(4), p 1908–1919
8. A. Shabani and M.R. Toroghinejad, Investigation of the Microstructure and the Mechanical Properties of Cu-NiC Composite Produced by Accumulative Roll Bonding and Coating Processes, *J. Mater. Eng. Perform.*, 2015, **24**(12), p 4746–4754
9. A. Shabani, M.R. Toroghinejad, and A. Shafyei, Fabrication of Al/Ni/Cu Composite by Accumulative Roll Bonding And Electroplating Processes and Investigation of Its Microstructure and Mechanical Properties, *Mater. Sci. Eng. A*, 2012, **558**, p 386–393

10. L. Ghalandari, M. Mahdavian, and M. Reihanian, Microstructure Evolution and Mechanical Properties of Cu/Zn Multilayer Processed by Accumulative Roll Bonding (ARB), *Mater. Sci. Eng. A*, 2014, **593**, p 145–152

11. M. Zabihi, M.R. Toroghinejad, and A. Shafyei, Shear Punch Test in Al/Alumina Composite Strips Produced by Powder Metallurgy and Accumulative Roll Bonding, *Mater. Sci. Eng. A*, 2016, **667**(Supplement C), p 383–390

12. C.A. León and R.A.L. Drew, Small Punch Testing for Assessing the Tensile Strength of Gradient Al/Ni-SiC Composites, *Mater. Lett.*, 2002, **56**(5), p 812–816

13. M. Zabihi, M.R. Toroghinejad, and A. Shafyei, Evaluating the Mechanical Behavior of Hot Rolled Al/Alumina Composite Strips Using Shear Punch Test, *Mater. Sci. Eng. A*, 2014, **618**, p 490–495

14. V. Karthik, K. Kasiviswanathan, K. Laha, and B. Raj, Determination of Gradients in Mechanical Properties of 2.25 Cr-1Mo Weldments Using Shear-Punch Tests, *Weld. J. N. Y.*, 2002, **81**(12), p 265

15. R. Alizadeh and R. Mahmudi, Evaluating High-Temperature Mechanical Behavior of Cast Mg-4Zn-xSb Magnesium Alloys by Shear Punch Testing, *Mater. Sci. Eng. A*, 2010, **527**(16), p 3975–3983

16. A. Geranmayeh, R. Mahmudi, and M. Kangooie, High-Temperature Shear Strength of Lead-Free Sn-Sb-Ag/Al2O3 Composite Solder, *Mater. Sci. Eng. A*, 2011, **528**(12), p 3967–3972

17. A. Shabani, M.R. Toroghinejad, and A. Shafyei, Effect of Post-Rolling Annealing Treatment and Thickness of Nickel Coating on the Bond Strength of Al-Cu Strips in Cold Roll Bonding Process, *Mater. Des.*, 2012, **40**, p 212–220

18. A. Shabani, M.R. Toroghineja, and A. Bagheri, Effects of Intermediate Ni layer on Mechanical Properties of Al-Cu Layered Composites Fabricated Through Cold Roll Bonding, *Int. J. Miner. Metall. Mater.*, 2018, **25**(5), p 573–583

19. L. Lutterotti, MAUD, Material Analysis Using Diffraction, *Copyright (c)*, 2008 (1997)

20. G. Dini, R. Ueji, A. Najafizadeh, and S. Monir-Vaghefi, Flow Stress Analysis of TWIP Steel Via the XRD Measurement of Dislocation Density, *Mater. Sci. Eng. A*, 2010, **527**(10), p 2759–2763

21. A. Chanda and M. De, X-ray Characterization of the Microstructure of α-CuTi alloys by Rietveld's Method, *J. Alloy. Compd.*, 2000, **313**(1), p 104–114

22. A. Shabani, M.R. Toroghinejad, A. Shafyei, and P. Cavaliere, Effect of Cold-Rolling on Microstructure, Texture and Mechanical Properties of an Equiatomic FeCrCuMnNi High Entropy Alloy, *Materialia*, 2018, **1**, p 175–184

23. M. Toloczko, M. Hamilton, and G. Lucas, Ductility Correlations Between Shear Punch and Uniaxial Tensile Test Data, *J. Nucl. Mater.*, 2000, **283**, p 987–991

24. L. Won-Bae, B. Kuek-Saeng, and J. Seung-Boo, Effects of Intermetallic Compound on the Electrical and Mechanical Properties of Friction Welded Cu/Al Bimetallic Joints During Annealing, *J. Alloy. Compd.*, 2005, **390**, p 212–219

25. M. Raei, M.R. Toroghinejad, R. Jamaati, and J.A. Szpunar, Effect of ARB Process on Textural Evolution of AA1100 Aluminum Alloy, *Mater. Sci. Eng. A*, 2010, **527**(26), p 7068–7073

26. R. Jamaati and M.R. Toroghinejad, Effect of Stacking Fault Energy on Deformation Texture Development of Nanostructured Materials Produced by the ARB Process, *Mater. Sci. Eng. A*, 2014, **598**, p 263–276

27. M.R. Toroghinejad, R. Jamaati, M. Hoseini, J.A. Szpunar, and J. Dutkiewicz, Texture Evolution of Nanostructured Aluminum/Copper Composite Produced by the Accumulative Roll Bonding and Folding Process, *MMTA*, 2013, **44**(3), p 1587–1598

28. L. Chen, Q. Shi, D. Chen, S. Zhou, J. Wang, and X. Luo, Research of Textures of Ultrafine Grains Pure Copper Produced by Accumulative Roll-Bonding, *Mater. Sci. Eng. A*, 2009, **508**(1-2), p 37–42

29. R. Jamaati, Unexpected Cube Texture in Cold Rolling of Copper, *Mater. Lett.*, 2017, **202**, p 111–115

30. F.J. Humphreys and M. Hatherly, *Recrystallization and Related Annealing Phenomena*, 2nd ed., Elsevier, Amsterdam, 2004

31. J.R. Davis, P. Allen, S. Lampman, T.B. Zorc, S.D. Henry, J.L. Daquila, and A.W. Ronke, *Metals Handbook: Properties and Selection: Nonferrous Alloys and Special-Purpose Materials*, ASM International, Geauga County, 1990

32. P.J. Hsieh, Y.P. Hung, and J.C. Huang, Transformation into Nanocrystalline or Amorphous Materials in Zr-X Binary Systems Using ARB Route, *Scr. Mater.*, 2003, **49**, p 173–178

33. M. Shamanian, M. Mohammadnezhad, and J. Szpunar, Production of High-Strength Al/Al2O3/WC Composite by Accumulative Roll Bonding, *J. Mater. Eng. Perform.*, 2014, **23**(9), p 3152–3158